Oxytocin Enables Maternal Behavior by Balancing Cortical Inhibition

Bianca J. Marlin[1,2,3,4], **Mariela Mitre**[1,2,3,4,5], **James A. D'amour**[1,2,3,4], **Moses V. Chao**[1,2,4,5,6], and **Robert C. Froemke**[1,2,3,4,6,*]

[1]Skirball Institute for Biomolecular Medicine, New York University School of Medicine, New York, NY, USA

[2]Neuroscience Institute, New York University School of Medicine, New York, NY, USA

[3]Department of Otolaryngology, New York University School of Medicine, New York, NY, USA

[4]Department of Neuroscience and Physiology, New York University School of Medicine, New York, NY, USA

[5]Departments of Cell Biology, Psychiatry, New York University School of Medicine, New York, NY, USA

[6]Center for Neural Science, New York University, New York, NY, USA

Abstract

Oxytocin is important for social interactions and maternal behavior. However, little is known about when, where, and how oxytocin modulates neural circuits to improve social cognition. Here we show how oxytocin enables pup retrieval behavior in female mice by enhancing auditory cortical pup call responses. Retrieval behavior required left but not right auditory cortex, was accelerated by oxytocin in left auditory cortex, and oxytocin receptors were preferentially expressed in left auditory cortex. Neural responses to pup calls were lateralized, with co-tuned and temporally-precise excitatory and inhibitory responses in left cortex of maternal but not pup-naive adults. Finally, pairing calls with oxytocin enhanced responses by balancing the magnitude and timing of inhibition with excitation. Our results describe fundamental synaptic mechanisms by which oxytocin increases the salience of acoustic social stimuli. Furthermore, oxytocin-induced plasticity provides a biological basis for lateralization of auditory cortical processing.

The neuropeptide oxytocin controls social behaviors such as pair bond formation, mating, and parenting[1–14]. Oxytocin is synthesized in the paraventricular nucleus (PVN) and supraoptic nucleus of the hypothalamus, and binds to a G protein-coupled receptor with a

single isoform[1–2]. Peripheral release of oxytocin is important for parturition and lactation[2,7,9], whereas central release of oxytocin appears to have cognitive effects including increased interpersonal trust and enhanced salience of socially-relevant sensory input[1,3,4,6,10]. However, it remains unclear which neurons express oxytocin receptors[15,16], or how oxytocin interacts with experience to modify neural circuits and increase the salience of social information.

Here we examine how oxytocin is involved in pup retrieval, an important form of mammalian social behavior. Mouse pups emit ultrasonic distress calls when separated from the nest, which experienced mothers ('dams') use to locate and retrieve isolated pups[17–23]. This behavior relies on the auditory system, as pup calls played by speakers attract maternal animals[19,21]. Physiologically, neural responses to pup calls in mouse auditory cortex differ between dams and virgin females, with higher signal-to-noise ratios in maternal mice[23–27]. Correspondingly, most inexperienced animals do not initially retrieve pups[28]. Intriguingly, some virgin female rodents start retrieving pups after being co-housed with dam and pups or after central administration of oxytocin[7]. An ethologically-important form of plasticity in auditory cortex might therefore be enabled by oxytocin in maternal animals, allowing them to recognize the behavioral significance of infant distress calls. Here we aim to show how these neural changes occur, and what role oxytocin plays in experience-dependent pup retrieval by virgins.

Oxytocin Enables Pup Retrieval Behavior

We first determined the time course of experience-dependent pup retrieval behavior enabled by oxytocin (Fig. 1a). Non-retrieving virgin female mice were co-housed with dams and litters, and retrieval success rates of virgins tested over 3–7 days. Mothers were first tested to ensure that they reliably retrieved pups (Fig. 1b, d; Supplementary Video 1). Three groups of virgins were examined for pup retrieval. The first group of wild-type virgins received systemic oxytocin injections before testing (Fig. 1b–d, red). The second wild-type group received saline vehicle injections (Fig. 1b–d, black). The third optogenetic group of *oxytocin-IRES-Cre* mice[29,30] ('*Oxt-IRES-Cre*') expressed channelrhodopsin-2 ChETA in PVN oxytocin neurons, with optical fibers implanted in PVN to enhance release of endogenous oxytocin and perhaps other co-factors during retrieval testing (Fig. 1b–d, blue; Extended Data Fig. 1).

Within 12 hours of being co-housed, virgin females receiving either oxytocin or optical PVN stimulation began retrieving more than saline-injected animals (Fig. 1b, c; Extended Data Fig. 2). Saline-injected virgins generally required 2+ days of co-housing to express retrieval behavior (Fig. 1b, c, black; Supplementary Video 2). Systemic oxytocin or optogenetic stimulation accelerated and increased retrieval, even sometimes after only a few hours of co-housing (Fig. 1b, c; Supplementary Video 3). Once retrieving, experienced virgin and dam retrieval rates and speeds were similar (Fig. 1d).

We examined retrieval in single-housed virgin females, to determine if effects of oxytocin required co-housing with dam and litter. Isolated virgins receiving oxytocin injections began retrieving earlier than saline-injected virgins, although slower than co-housed virgins (Fig.

1e). This demonstrates that oxytocin enables retrieval in single-housed virgins, specifically during interactions with isolated pups.

Oxytocin Receptor Expression Is Lateralized

Where in the brain might oxytocin be acting to improve social cognition and enable maternal behavior? While peripheral oxytocin injections or nasal sprays has pro-social effects, it remains unclear how and where oxytocin acts on neural circuits[1,6] outside recent studies in transgenic mice[15,16]. To determine which cells express oxytocin receptors, we generated a specific antibody, OXTR-2 (Fig. 2a). The antibody labeled a subset of cells in auditory cortex and other areas (Fig. 2b, Extended Data Fig. 3) enriched for oxytocin and oxytocin receptors[2,3,31]. Cells were unlabeled in oxytocin receptor knockout animals[32] (Fig. 2c, Extended Data Fig. 3). We confirmed expression patterns in bacterial artificial chromosome (BAC) transgenic oxytocin receptor-eGFP mice[16,33] using antibodies to GFP (Fig. 2d). ~30–40% of parvalbumin-positive (PV+) and somatostatin-positive (SST+) inhibitory interneurons expressed oxytocin receptors (Fig. 2e, f), suggesting that oxytocin is important for controlling cortical inhibition[15,16]. We also observed YFP-positive PVN axons in auditory cortex of *Oxt-IRES-Cre* mice after viral injection, demonstrating that hypothalamic oxytocin neurons project to cortex (Extended Data Fig. 4a–c).

Surprisingly, receptor expression in female auditory cortex was lateralized (Fig. 2g). Significantly more cells expressed oxytocin receptors in left auditory cortex compared to right auditory cortex in mothers and naive virgins (Fig. 2h). Left auditory cortex might therefore be especially sensitive to oxytocin modulation and specialized for processing social stimuli such as pup calls. As axonal projections from PVN into cortex were not obviously lateralized (Extended Data Fig. 4d), it is likely that this anatomical specialization emerges within cortex.

Retrieval Requires Left Auditory Cortex

We next asked if left auditory cortex was functionally important for pup retrieval. We implanted cannulas into left or right primary auditory cortex (AI) of inexperienced virgins or dams. First, we unilaterally infused the GABA agonist muscimol to transiently inactivate left or right auditory cortex prior to behavioral testing. Muscimol in left but not right auditory cortex impaired retrieval (Fig. 3a, b, Supplementary Video 4), showing that activity in left auditory cortex is required for retrieval. These data extend an earlier study using unilateral ear plugs to show that maternal animals have right ear/left brain advantage for recognizing pup call sounds[19].

We wondered if oxytocin within virgin left auditory cortex might accelerate expression of retrieval. Although it is unlikely that activation of a single brain area is entirely sufficient for retrieval, sensitization of left AI might be critical for recognizing the significance of distress calls. Animals receiving oxytocin or optogenetically stimulated in left auditory cortex began retrieving earlier than saline-infused animals (Fig. 3c, Supplementary Video 5,6). Thus left auditory cortex is a major component of oxytocin-sensitive circuitry for maternal behavior.

We then asked if oxytocin receptor activation itself was required for behavioral performance in experienced animals. We used antagonists of oxytocin receptors (OTA or L-368,899) infused into left auditory cortex before testing retrieval in experienced animals. Neither antagonist affected performance (Fig. 3d). These data suggest that oxytocin receptors might be required only when animals first begin to retrieve, but are unnecessary for expression of retrieval behavior thereafter (analogous to requirement of NMDA receptors for LTP induction but not maintenance). Thus after experience with pup calls during heightened cortical oxytocin levels, changes are induced in left auditory cortex to enable enduring memory traces for maternal behavior.

Responses to Pup Calls in Cortical Neurons

We then asked what circuit modifications in auditory cortex are enabled by oxytocin. Our goal was to first characterize pup call responses in single neurons from maternal animals, before determining synaptic mechanisms by which oxytocin affects the virgin brain. We used *in vivo* whole-cell recordings[34–37] to measure AI pup call responses in isoflurane-anesthetized dams, naïve virgins, and experienced virgins. In 21 current-clamp and 37 cell-attached recordings, pup calls evoked stronger responses in left AI of mothers and experienced virgins than in naïve virgins (Fig. 4a–c). As responses to pure tones were comparable across groups (Fig. 4d), differences in responsiveness between experienced and inexperienced females are specific for pup calls, not simply due to more auditory-responsive neurons in maternal cortex. Responses in experienced females were lateralized to left AI (Extended Data Fig. 5a, b). Surprisingly, calls evoked precise spikes in maternal animals but not naive virgins (Fig. 4e) or right AI (Extended Data Fig. 5a, b). We quantified temporal similarity by computing trial-to-trial cross-correlation for spiking responses, finding higher correlations in left AI neurons from experienced females (Fig. 4e; Extended Data Fig. 5b).

To examine synaptic responses to pup calls, we made 58 *in vivo* voltage-clamp recordings from AI neurons. Substantial excitatory and inhibitory postsynaptic currents (EPSCs/ IPSCs) were evoked by calls in all animals. Amplitudes of call-evoked synaptic responses (Fig. 5a, b), tone-evoked responses (Fig. 5c), and spontaneous activity (Extended Data Fig. 6a–d) were comparable across groups, suggesting that reliable call-evoked spiking in maternal left AI could not be explained simply by these neurons receiving stronger excitatory inputs.

Instead, excitation and inhibition were balanced (co-tuned and precisely timed) in left AI neurons of experienced females but not naive virgins or right AI. We quantified degree of excitatory-inhibitory balance of call-evoked responses three ways: trial-by-trial similarity in patterns of excitatory or inhibitory responses (r_e, r_i), fine-scale correlation of temporal structure between EPSCs and IPSCs from best calls ($r_{ei-best}$), and overall correlation between EPSC and IPSC amplitudes across all calls (r_{ei-all}). First, we examined synaptic responses to best calls, and found that in experienced animals, patterns of EPSCs and IPSCs were similar and more reliable from trial-to-trial (Extended Data Fig. 6b, e).

For fine-scale excitatory-inhibitory balance, we observed that temporal profiles of call-evoked excitation and inhibition were almost identical in maternal animals. Although we could not simultaneously measure both excitation and inhibition in a given trial, we

reasoned that because of similarity between excitation and inhibition alone, average responses would also be correlated. Indeed, temporal correlations of EPSCs and IPSCs evoked by best calls ($r_{ei-best}$) were higher in left AI of experienced animals (Fig. 5d, Extended Data Fig. 5c). Finally, for overall correlation across vocalizations, each different call evoked a distinct EPSC/IPSC pattern. In left AI neurons from experienced but not naive animals, call-evoked EPSC and IPSC magnitudes were correlated (Fig. 5d, Extended Data Fig. 5c).

Temporal correlation of excitation and inhibition provides a mechanism for reliable and precisely-timed spiking responses. As proof of principle, we simulated spiking evoked by different sets of synaptic call-evoked responses in a conductance-based integrate-and-fire model neuron[36]. We computed membrane potential and spiking responses and observed precisely-timed spikes in cells from experienced but not naïve animals (Extended Data Fig. 7), due to temporal mismatch between excitation and inhibition. Therefore the patterns of EPSCs and IPSCs in experienced animals can account for reliable spiking observed in the maternal state.

Oxytocin Modulation and Plasticity of Pup Call Responses

Finally, we wondered how oxytocin sensitized neural circuits of virgin left AI to pup calls, to enable reliable spiking and successful retrieval in initially-inexperienced animals. First we examined neuromodulatory effects of oxytocin on cortical responses in vivo and in vitro. In voltage-clamp recordings, oxytocin reduced call-evoked IPSCs within seconds (Fig. 6a, b, open; Extended Data Fig. 8). In contrast, EPSCs were gradually modified over minutes (Fig. 6a, b, filled). Therefore, oxytocin rapidly disinhibits auditory cortex much like acetylcholine[37–40], suggesting that oxytocin may regulate attention and increase the salience of social stimuli. These results corroborate recent findings in hippocampal slices on the effects of oxytocin[41] and estrogen[42].

We then asked whether repetitive pairing of pup calls in the presence of oxytocin would persistently modify cortical pup call representations, effectively changing the virgin state into the maternal state. After recording responses to pup calls in virgin left AI, we paired calls for 3–5 minutes with either topical oxytocin application ('oxytocin pairing') or optical stimulation of AI in *Oxt-IRES-Cre* animals ('optogenetic pairing'). A recording demonstrating oxytocin pairing is shown in Figure 6c (individual trials in Extended Data Figure 9a). Before pairing, calls evoked unreliable EPSCs and IPSCs. During and after pairing, IPSCs decreased while EPSCs potentiated, becoming more reliable. 45 minutes after pairing, however, IPSCs increased in strength and reliability, balancing the temporal profile of inhibition with excitation.

To examine the slower dynamics of inhibitory plasticity after pairing, we made multiple recordings in series after the first recording[36,37]. The correlation of average excitation and inhibition evoked by paired calls ($r_{ei-paired}$) steadily increased over an hour and was stable thereafter (Fig. 6d). As excitatory modifications and changes in reliability were maximal after 20–30 minutes, this increase in excitatory-inhibitory balance likely reflects gradual

inhibitory potentiation, also evident in changes to inhibitory trial-by-trial correlations after pairing (Extended Data Fig. 9b).

Our simulations (Extended Data Fig. 7) indicated that this delayed balancing of excitation and inhibition has substantial consequences for call-evoked spiking. Specifically, spike timing precision should increase when IPSCs match the pattern of EPSCs. Consistent with this hypothesis, spiking responses were rapidly increased during and after pairing, but trial-by-trial correlations increased only after an hour (Fig. 6f). Thus, briefly pairing pup calls with cortical oxytocin triggers long-lasting changes in virgin AI circuitry, balancing inhibition with excitation to enhance call representation and perceptual salience within minutes to hours.

Discussion

Our results demonstrate a remarkable degree of functional lateralization in the mammalian brain and provide a molecular basis for this phenomenon. Left auditory cortex is specialized for recognizing the behavioral significance of infant distress calls and required for maternal retrieval of isolated pups. This is strikingly similar to the asymmetry of speech processing in human temporal lobe[43,44], and supports earlier behavioral observations of auditory lateralization in maternal mice[19]. We generated an antibody to the mouse oxytocin receptor, OXTR-2, and found more receptor expression in left auditory cortex. A dedicated neural circuit, enriched for oxytocin receptors, might therefore be specialized for processing important social signals such as pup distress calls. This specialization would allow maternal animals to rapidly and reliably attend to their young and return pups to the nest. Furthermore, given the importance of olfactory signals in social behaviors including pup retrieval[13,23,45,46], it is likely that oxytocin also enhances olfaction[47] in combination with other cues (e.g., pup calls) to synergistically improve parenting behavior.

Although many aspects of mammalian maternal behavior may be innate[48–50], recognition of the behavioral importance of pup calls depends on experience[21,23,25–28]. Several studies highlight differences between AI responses in maternal and pup-naive female mice. In particular, pup call responses have been found to be less reliable in pup-naive virgins[23,25–27]. Our results directly demonstrate how oxytocin paired with pup calls rapidly changes brain state, transforming weaker virgin responses into more robust and temporally precise maternal-like responses. The predominant effect of oxytocin is to reduce cortical inhibition within seconds, followed by longer-term modifications over hours hypothesized to be essential for balancing inhibition with excitation, enhancing spiking, and successful maternal care. These synaptic dynamics are analogous to the imbalance of excitation and inhibition for tone-evoked responses in AI during early development when animals have had limited acoustic exposure[36]. After experience, however, tone-evoked excitation and inhibition become balanced over the first few weeks of life[34–37]. Our findings complement recent studies of neural circuits involved in social behavior[23,48–50] by revealing how ethologically-important behaviors with innate components can be quickly shaped and improved by experience. This may exemplify a general mechanism of neuromodulation for social behavior.

Methods

Behavior

All procedures were approved under NYU IACUC protocols. For measuring pup retrieval, we used 2–4 month-old C57BL/6 mothers or pup-naïve virgin female mice. Dams were initially pre-screened to ensure they retrieved pups; ~1% of dams did not retrieve pups and these animals were not used for co-housing. Naïve virgins were initially pre-screened for retrieval or pup mauling before co-housing; <30% of naïve virgins retrieved at least one pup or mauled pups during pre-screening and these animals were excluded from subsequent behavioral studies.

Each session of testing consisted of a baseline set of 10 trials and a post-injection/infusion set of 10 trials. For baseline testing, animals were placed in a behavioral arena (38×30×15 cm) containing nesting material. Animals were given at least 20 minutes to acclimate before each testing session began. Three to six pups ranging from postnatal day 1–4 were grouped in a corner of the arena and covered with nesting material. One pup was removed from the nest and placed in an opposite corner of the arena. The experimental female was given ten trials (two minutes per trial) to retrieve the displaced pup and return it back to the nest; if the displaced pup was not retrieved within two minutes, the pup was returned to the nest and the trial was scored as a failure. If the pup was successfully retrieved, the time to retrieval was scored. Another pup was then taken out of the nest, placed in an opposite corner, and the next trial was begun. After ten trials, pups were placed back into their home cage with their dam. We used an ultrasonic microphone (Avisoft) to verify that isolated pups vocalized during testing.

For post-injection testing (Fig. 1b–e), virgin females were injected intraperitoneally (IP) with oxytocin (20–50 μM in saline, 0.3 ml) or saline (0.3 ml). For post-infusion testing (Fig. 3c), cannulated virgin animals were infused with oxytocin (50 μM in saline, 1.5 μl at 1 μl/min) or saline (1.5 μl at 1μl/min). For animals that were co-housed (Fig. 1b–d), the dam and litter were placed in the arena with the experimental virgin female and the experienced dam was given at least 5–10 minutes to re-acclimate. Wild-type naive virgins were randomly assigned to different groups (saline or oxytocin, co-housed or isolate) by an experimenter blind to results of data analysis. Dam retrieval rates were tested in the presence of the experimental virgin female. Afterward, the dam was removed to her home cage and the retrieval rates of the virgin female were reassessed. Virgin female retrieval was then tested as described above, and afterward the virgin female was returned to her home cage with dam and pups. Best retrieval performance in Figure 1d was determined from the session with the highest retrieval rate and the session with the fastest retrieval time over all sessions for each animal. Isolated animal retrieval (Fig. 1e) was examined in absence of an experienced dam. The isolated virgin females were housed separately from dams and pups, and did not come into contact with the dams. Retrieval was tested at the following time points: 1, 3, 6, 12, 18, 24, 36, 48, and 72 hours. Power analysis was performed to determine sample size for statistical significance with a power of β:0.7; these studies required at least six animals, satisfied in the experiments of Figure 1. Fisher's two-tailed exact test was used for comparing numbers of animals retrieving in each group for Figures 1c and 1e as these data

were binomial, and Bonferroni correction used to adjust p-values for multiple comparisons. Comparisons were made relative to performance of saline-injected virgin females. ANOVA was used to compare retrieval performance in experienced animals in Figure 1d.

For testing the effects of muscimol or oxytocin receptor antagonist infusion, experienced retrievers were placed in the behavioral arena. Animals were given at least 5–10 minutes to re-acclimate, and baseline retrieval was performed as above. The animal was then infused with muscimol (2.5 mM in saline, 1.5 μl at 1 μl/min; Fig. 3a, b) or an oxytocin receptor antagonist[51,52]: either OTA (1 μM in saline, 1.5 μl at 1 μl/min; Fig. 3d, pink line, open circles) or L-368,899 (2.5 mM in saline, 1.5 μl at 1μl/min; Fig. 3d, purple line, filled circles). Mice were randomly assigned to different pharmacological groups by an experimenter blind to results of data analysis. Retrieval was reassessed following the infusion. After 24 hours, the experimental female was given 10 baseline trials, infused with saline (1.5 μl at 1 μl/min), and retrieval re-assessed following the infusion ('Post' testing). Power analysis was performed to determine sample size for statistical significance with a power of β:0.7; these studies required at least six animals, satisfied in the experiments of Figure 3. Wilcoxon's signed-rank matched-pairs tests were used to non-parametrically compare retrieval performance in Figure 3a, b, d. For comparing number of animals retrieving overall, Fisher's exact test was used (two-tailed for Figure 3c; one-tailed for Figure 3a, as all animals initially retrieved and the number of animals retrieving could only stay the same or decrease), comparing oxytocin/optogenetic animals to saline-infused virgin performance.

Stereotaxic viral injections were performed in *Oxy-IRES-Cre* mice[29,30]. Mice were anesthetized with 0.7–2.5% isoflurane, placed into a stereotaxic apparatus, and a craniotomy performed over PVN (from bregma: 0.72 mm posterior, 0.12 mm lateral, 4.5 mm ventral). Injections were performed with a 5 μL Hamilton syringe and a 33 gauge needle. Cre-inducible pAAV5-EF1α:-DIO-ChETA-EYFP virus[53] was injected into PVN 0.1 nl/s for a final injection volume of 1.2–1.5 μl. An optical fiber ferrule was then implanted either in PVN (4.5 mm ventral) or in electrophysiologically-identified AI (100 μm ventral). The craniotomy and implant was sealed with dental cement, and the virus was given a minimum of two weeks to express.

Production of oxytocin receptor antibodies

A custom peptide was synthesized based on the mouse oxytocin receptor amino acid sequence: EGSDAAGGAGRAALARVSSVKLISKAKI (amino acids 243–270) in the third intracellular loop[54]. This peptide was chosen based on a high level of antigenicity using the Thermo Scientific Antigen Profiler and lack of cross-reactivity. The resulting polyclonal antisera were tested using Western blot and immunohistochemistry before being further purified using affinity chromatography.

Specificity was tested via immunohistochemistry in wild-type and oxytocin receptor knockout[32] brain sections and via Western blot analysis of HEK293 cells (Invitrogen) expressing oxytocin receptors (pAAV-OXTR plasmid provided by L.J. Young, Emory) and protein extracts from mouse brain. HEK cells were tested for mycoplasma around time of use (mid-2013). Lysates were immunoprecipitated and immunoblotted with OXTR-2 to further evaluate specificity of antibody.

For immunohistochemical analysis, wild-type or oxytocin receptor knockout mice were anesthetized via IP injection (0.1 ml per 10 g) of a ketamine-xylazine mixture containing 15 mg/ml ketamine and 5 mg/ml xylazine in 0.9% sodium chloride solution. Mice were perfused intracardially with a solution of heparin (1000 units/ml) and phosphate buffered saline (PBS) to prevent clotting, followed by 40 ml per mouse of freshly-prepared 4% paraformaldehyde in PBS. After cryoprotection, sections were blocked and incubated with oxytocin receptor primary antibody diluted in PBS to a concentration of 1 μg/ml. Sections were incubated for two days at 4C in a moist chamber. Sections were washed with PBS (3 × 15 min at room temperature) in a staining jar and incubated for 1–2 hours at room temperature in Alexa fluor-conjugated secondary antibodies diluted 1:500 in PBS. Unbound secondary antibodies were washed with PBS (3 × 15 min at room temperature) and sections were incubated for 10 min at room temperature with a Hoechst solution (1:10000 stock diluted in PBS) for nuclear staining. After a final rinse, the slides were cover-slipped using fluoromount G (Southern Biotechnology Associates, Inc.). The brains of wild-type and knockout animals were processed together to minimize confounding factors, and parallel sections from knockout animals served as controls. For inhibitory marker co-staining, the protocol followed the procedures described above with the addition of a parvalbumin primary antibody (mouse anti-parvalbumin, Swant, 235, 1:1000) and a somatostatin primary antibody (rat anti-somatostatin, Millipore, MAB354, 1:1000) in the oxytocin receptor antibody solution. The secondary antibodies used in these experiments were donkey anti-rabbit Alexa 488 (Molecular Probes; 1:500), donkey anti-rat Alexa 555 (Molecular Probes; 1:500), donkey anti-mouse Alexa 647 (Molecular Probes; 1:500). As a control, omission of primary antibody and/or pre-incubation with peptide eliminated immunofluorescent labeling.

Anatomy

Oxytocin receptor-eGFP mice were created by the GENSAT initiative from a BAC clone containing EGFP upstream of oxytocin receptor gene[16,33]. Cryopreserved embryos of this line were imported from the Mutant Mouse Regional Resource Centers (MMRRC) and rederived by the NYU transgenic mouse core facility. These mice were on an FVB/N-Swiss Webster background and were bred by mating hemizygous males with wild-type females. Wild-type littermates were used as controls for GFP antibody staining. The animals were genotyped using a strain-specific protocol provided by the MMRRC using the following primers: OXTR forward: GCCACACTTTAAAGAGCCTCAA; GFP reverse: TAGCGGCTGAAGCACTGCA. Note that not all cells natively expressing oxytocin receptors necessarily express the transgene, due to ectopic expression or lack of regulatory elements[55].

Slides were examined and imaged using a Carl Zeiss LSM 700 confocal microscope with four solid-state lasers (405/444, 488, 555, 639 nm) and appropriate filter sets. For imaging sections co-stained with multiple antibodies, we used short-pass 555 nm (Alexa Fluor 488), short-pass 640 nm (Alexa Fluor 555), and long-pass 640 nm (Alexa Fluor 647) photomultiplier tubes. The distribution and number of immunoreactive cells in each section were determined by taking images of wild-type and knockout sections under the same laser power output, pinhole aperture, and gain. Images of left and right auditory cortex in at least

3 sections per brain were collected and saved for manual counts by two independent blinded observers. Mean numbers of labeled cells were calculated and compared in Figure 2h by Student's paired two-tailed t-tests as data passed Kolmogorov-Smirnov normality tests. Power analysis was performed to determine sample size for statistical significance with a power of β:0.7; these studies required at least seven animals, satisfied in the experiments of Figure 2h. Images of sections costained with inhibitory interneuron markers were collected for each channel and merged to evaluate colocalization with oxytocin receptors by two independent blinded observers. For axon length measurements in Extended Data Figure 4d, YFP-positive axon segments from left and right auditory cortex sections in *Oxt-IRES-Cre* animals were quantified with ImageJ by one blinded observer. Four sections spanning anterior to posterior auditory cortex from each animal and each cortical area were examined, and confocal images consisted of a z-stack that spanned the thickness of the section. Axon counts were averaged together across the four sections from each animal, and average counts tested for statistical differences with an unpaired two-tailed Student's t-test.

Surgical preparation

For *in vivo* electrophysiology or implanting cannulas/ferrules into auditory cortex, female mice were anesthetized with isoflurane (0.5–2.5%). A small craniotomy was performed over left or right auditory cortex with stereotaxic coordinates (from bregma in mm: 2.9 posterior, 4.0 lateral). To ensure recordings or implants were targeted to AI, we first recorded multiunit activity with tungsten electrodes. AI was mapped with pure tones (60 dB SPL, 7–79 kHz, 50 msec, 1 msec cosine on/off ramps) delivered in pseudo-random sequence at 0.5–1 Hz. For survival surgeries, a cannula or ferrule was then implanted (0.6 mm projection, dummy 0.6 mm projection, internal 0.7 mm projection) using dental acrylic, and animals were given 3–7 days to recover before behavioral testing.

For viral injections, *Oxt-IRES-Cre* animals were bred into a C57BL/6 background. Female mice 2–4 months old were anesthetized with isoflurane (0.5–2.5%). A craniotomy was performed over the left PVN using stereotaxic coordinates (from bregma in mm: 0.7 posterior, 0.25 lateral, 4 ventral), and pAAV5-Ef1a-DIO-ChETA-EYFP (1–1.2 μl) was injected (0.1 μl/min). Animals were given at least two weeks to recover to allow adequate expression of the ChETA variant of channelrhodopsin-2.

Electrophysiology

In vivo recordings were performed in a sound-attenuating chamber. Initially, auditory cortex was mapped with multi-unit recordings using a tungsten electrode to determine the tonotopic organization of the primary field AI[24]. After locating AI, *in vivo* whole-cell recordings[34–37] were made from AI neurons with a Multiclamp 700B amplifier (Molecular Devices). For current-clamp recordings, patch pipettes (4–9 MΩ) contained (in mM): 115 K-gluconate, 20 KCl, 1.5 MgCl2, 10 HEPES, 10 phosphocreatine, 2 MgATP, 0.5 NaGTP, pH 7.3. For voltage-clamp recordings, pipettes contained: 130 Cs-methanesulfonate, 1 QX-314, 4 TEA-Cl, 0.5 BAPTA, 4 MgATP, 20 phosphocreatine, 10 HEPES, pH 7.2. Whole-cell recordings from AI neurons were obtained from cells located 420–800 μm below the pial surface. Data were filtered at 5 kHz, digitized at 20 kHz, and analyzed with Clampfit 10 (Molecular Devices). Resting potential of AI neurons: –65.4±14.7 mV; Rs: 33.1±24.4 MΩ; Ri:

186.1±83.1 MΩ (s.d.). Recordings were excluded from analysis if R_s or R_i changed >30% compared to the baseline period.

Pup calls were recorded from isolate pups with an ultrasonic microphone, and a library of six calls (1 s duration, maximal intensity of 60 dB SPL) was used for measuring pup call responses. For measuring spiking responses, cell-attached recordings were first high-pass filtered at 100–200 Hz. Spikes were automatically detected in current-clamp or cell-attached recordings by threshold crossing in Clampex 10. Pure tones (50 msec duration, 3 msec cosine on/off ramps) over 4–64 kHz (0.2–1.0 octave steps) were played at 60 dB SPL. Tone-evoked responses were measured in a 50 msec window starting at tone onset and compared to spontaneous activity in the 50 msec before tone onset. Call-evoked responses were measured throughout the call duration plus 200 msec, and compared to spontaneous activity in the 500 msec before call onset, normalized by computing the z-scored call-evoked firing rate relative to the spontaneous rate: $z = (\mu_{evoked} - \mu_{spontaneous})/\sigma_{spontaneous}$. Response magnitude in Figures 4 and 5 are shown for the best frequency and best call, where 'best' is defined as the stimulus that evoked the maximal amount of spiking or excitatory current.

For measuring trial-by-trial similarity of spike trains[56], binary spike trains were smoothed by convolution with a Gaussian filter (σ: 10 msec) and trial-by-trial cross-correlations computed (~10–20 trials/call/cell); all pairwise cross-correlations were then averaged to measure r for spiking responses in Figures 4 and 6, and Extended Data Figure 5. In raster plots of Figure 4 and Extended Data Figure 7, yellow events are simply illustrative and indicate spikes that are synchronous within ~10 msec on 50%+ trials. Synaptic responses and trial-by-trial correlations were measured in a similar manner for Figures 5 and 6, and Extended Data Figures 5, 6, and **9**, except that responses were measured as the instantaneous current (in pA): the current integral from call onset to 200 msec after call onset (in pA*msec) and divided by the total time (in msec). Synaptic responses were not smoothed before computing zero-lag cross-correlations between all pairs of individual trials. For examining changes in spiking responses and spiking or synaptic correlations over multiple cells in Figure 6 and Extended Data Figure 9, measurements were made up to one hour before pairing, and at 10, 30, 45, and 60 minutes post-pairing when possible. Measurements at longer time periods were made whenever subsequent whole-cell recordings were obtained, separated by at least 15 min/cell thereafter.

For Figure 4 and 5, and Extended Data Figures 5–7, statistics and error bars are reported as medians±interquartile range for spiking and synaptic responses to pup calls. As these data did not all pass Kolmogorov-Smirnov normality tests, non-parametric Wilcoxon-Mann-Whitney two-sample rank tests were used for comparing pup call responses in experienced animals to virgin animal responses (however, we note that p-values obtained with Student's two-tailed unpaired t-tests were similar, and each of the significant differences reported here were significant under both parametric and non-parametric statistics). Power analysis was performed to determine sample size for statistical significance with a power of β:0.7; these studies required at least seven neurons for differences in spiking and at least four neurons for differences in synaptic correlations, satisfied in the experiments of Figure 4 and 5, and Extended Data Figures 5 and 6.

For pairing pup calls with exogenous oxytocin, baseline responses to pup calls were recorded for 5–20 minutes. A non-preferred pup call was then presented for 1–5 minutes at 0.5–1 Hz in the presence of topically-applied oxytocin (50 μM). For pairing calls with endogenous oxytocin release via optogenetic stimulation in *Oxt-IRES-Cre* mice, blue light pulse trains (473 nm wavelength, 10 ms pulse width duration, 30 Hz stimulation frequency, 1 s total pulse train duration) were delivered (final output powers: 10–15 mWmm^{-2} at brain surface). Pup call presentation began at optical pulse train onset. Changes in responses in Figure 6 and Extended Data Figure 9 were compared by Student's paired two-tailed t-tests as data passed Kolmogorov-Smirnov normality tests. Power analysis was performed to determine sample size for statistical significance with a power of β:0.7. Modulation experiments of Figure 6b required at least three neurons for each group, plasticity experiments of Figure 6d required at least nine neurons for oxytocin pairing and four neurons for optogenetic pairing, and studies of synaptic and spiking correlations of Figure 6d,f and Extended Data Figure 9b required at least eleven neurons; these were all satisfied in the experiments of Figure 6 and Extended Data Figure 9.

In vitro recordings were performed in auditory cortex slices prepared from adult C57Bl/6 wild-type or *Oxt-IRES-Cre* mice. Animals were deeply anesthetized with a 1:1 ketamine/xylazine cocktail and decapitated. The brain was rapidly placed in ice-cold dissection buffer containing (in mM): 87 NaCl, 75 sucrose, 2 KCl, 1.25 NaH$_2$PO$_4$, 0.5 CaCl$_2$, 7 MgCl$_2$, 25 NaHCO$_3$, 1.3 ascorbic acid, and 10 dextrose, bubbled with 95%/5% O$_2$/CO$_2$ (pH 7.4). Slices (300–400 μm thick) were prepared with a vibratome (Leica), placed in warm dissection buffer (33–35°C) for <30 min, then transferred to a holding chamber containing artificial cerebrospinal fluid at room temperature (ACSF, in mM: 124 NaCl, 2.5 KCl, 1.5 MgSO$_4$, 1.25 NaH$_2$PO$_4$, 2.5 CaCl$_2$, and 26 NaHCO$_3$,). Slices were kept at room temperature (22–24°C) for at least 30 minutes before use. For experiments, slices were transferred to the recording chamber and perfused (2–2.5 ml min^{-1}) with oxygenated ACSF at 33°C. Whole-cell voltage-clamp recordings were made from layer 5 pyramidal cells with an Multiclamp 700B amplifier (Molecular Devices) using IR-DIC video microscopy (Olympus). Patch pipettes (3–8 MΩ) were filled with intracellular solution (in mM: 130 Cs-methanesulfonate, 1 QX-314, 4 TEA-Cl, 0.5 BAPTA, 4 MgATP, 20 phosphocreatine, 10 HEPES, pH 7.2). Data were filtered at 2 kHz, digitized at 10 kHz, and analyzed with Clampfit 10 (Molecular Devices). Recordings were excluded from analysis if R$_s$ or R$_i$ changed >30% compared to baseline. Focal extracellular stimulation (0.01–1.0 msec, 5–150 μA) was applied with a bipolar glass electrode 100–150 μm from the recording electrode. Mean peak IPSCs were measured in a 5–10 msec window. Changes in IPSCs were compared by Student's unpaired two-tailed t-tests as data passed Kolmogorov-Smirnov normality tests. Power analysis was performed to determine sample size with a power of β:0.6; these studies required at least three neurons, satisfied in the experiments of Extended Data Figure 8d.
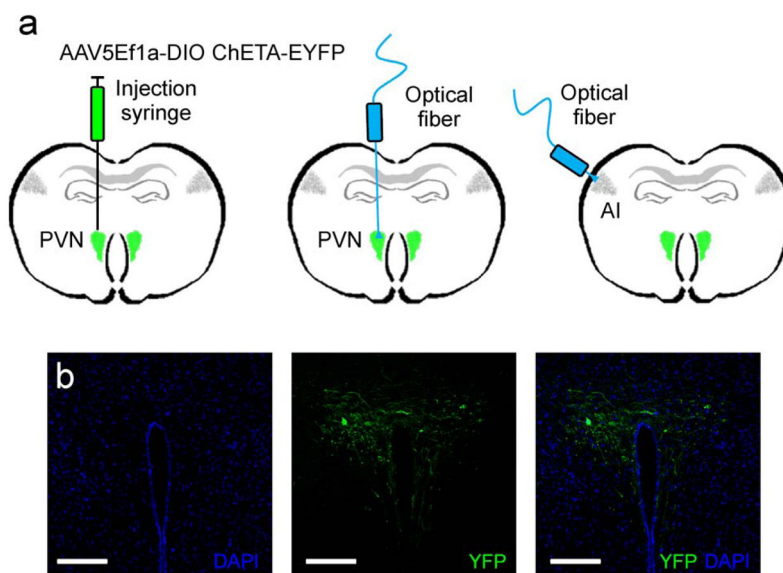
Simulations

The simulations in Extended Data Figure 7 used a conductance-based integrate-and-fire model neuron similar to our previous study relating synaptic currents and spike generation[36]. For simulating the spiking patterns of each cell, we used EPSCs and IPSCs from Figure 5b. On each trial, one 1.4 second EPSC and one 1.4 second IPSC were

randomly chosen from the set of recorded responses. Excitatory and inhibitory synaptic conductances g_e and g_i were computed from currents as previously described[34–37], and then g_e and g_i were randomly rescaled on each trial to have peak instantaneous conductance over the range 1.0–1.7 nS. Membrane voltage was dV computed as:

$$\tau_m \frac{dV}{dt} = V_{rest} - V + g_e(t)(E_e - V) + g_i(t)(E_i - V),$$

with τ_m=10 msec, resting dt membrane potential V_{rest}= −70 mV, excitatory reversal potential E_e=0 mV, and inhibitory reversal potential E_i= −70 mV. A spike was evoked in the postsynaptic neuron if the membrane voltage reached threshold of −40 mV, at which point the membrane potential was set to −80 mV in the next time step. Spike rates and trial-by-trial correlation were determined over 25 trials (approximately the number of trials used for measuring these values in the experiments), and twelve representative trials displayed in Extended Data Figure 7a–c for each simulation. Code can be obtained at: http://froemkelab.med.nyu.edu/marlin_etal_simulations.

Extended Data

Extended Data Figure 1.
Expression of ChETA in oxytocinergic PVN neurons of *Oxt-IRES-Cre* animals. **a,** Preparation of *Oxt-IRES-Cre* mice for optogenetic stimulation of endogenous oxytocin release. Animals had an AAV expressing the ChETA variant of channelrhodopsin-2 and YFP (AAV5Ef1a-DIO ChETA-EYFP) stereotaxically injected into left PVN (left) and cannulas for fiber optic stimulation implanted either in PVN (middle) or left AI (right). **b,** Confirmation of viral expression in PVN. Green, YFP. Blue, DAPI. Scale, 100 μm.
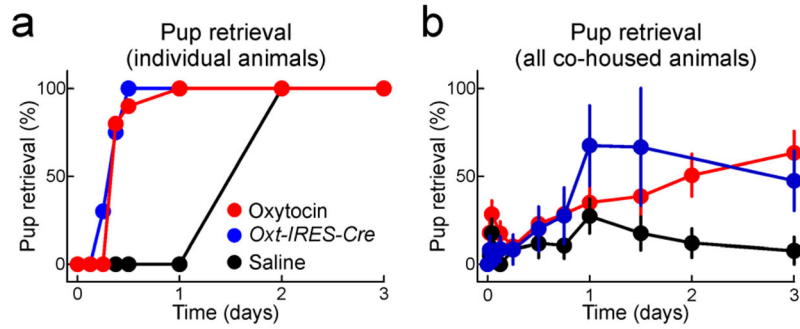
Extended Data Figure 2.
Retrieval success rates over time. **a**, Examples of retrieval rate from three different virgin females receiving optogenetic stimulation of PVN (blue), oxytocin injections (red), or saline injections (black). Each data point is the average over 10 two-minute trials immediately after injection or optical stimulation. **b**, Mean retrieval success at each time point for all co-housed virgin animals (including those that never retrieved within the first three days of co-housing). Some animals that began retrieving at earlier time points were not assessed at later time points and instead used for electrophysiological experiments.
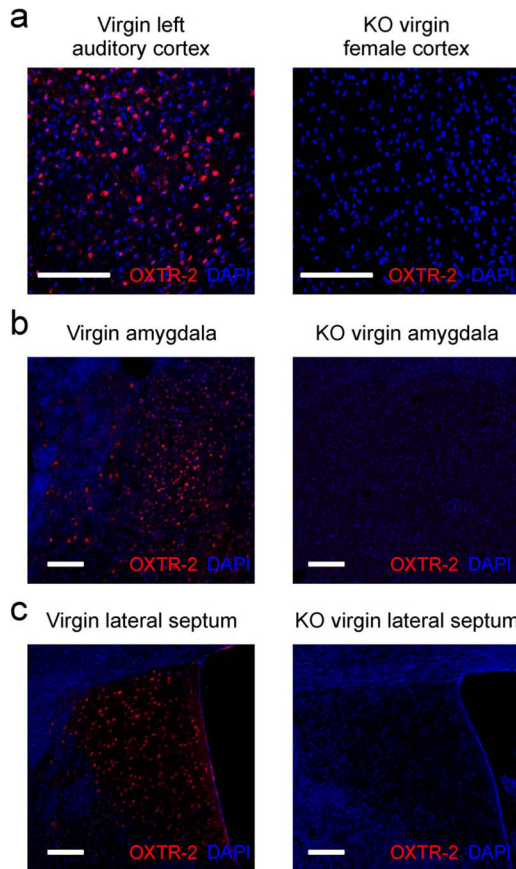
Extended Data Figure 3.

Oxytocin receptor expression in virgin female mouse auditory cortex, amygdala, and lateral septum. OXTR-2 labeling was detected in each area in wild-type but not oxytocin receptor knockout animals. **a**, Oxytocin receptor expression measured with OXTR-2 immunostaining in layer 5 of left auditory cortex of naïve wild-type animal (left) or oxytocin receptor knockout animal (right) imaged at 20X. Red, OXTR-2; blue, DAPI. Scale, 100 μm. **b**, OXTR-2 immunostaining in amygdala of wild-type animal (left) or oxytocin receptor knockout animal (right) imaged at 10X. Scale, 100 μm. **c**, OXTR-2 immunostaining in lateral septum of wild-type animal (left) or oxytocin receptor knockout animal (right) imaged at 10X. Scale, 100 μm.
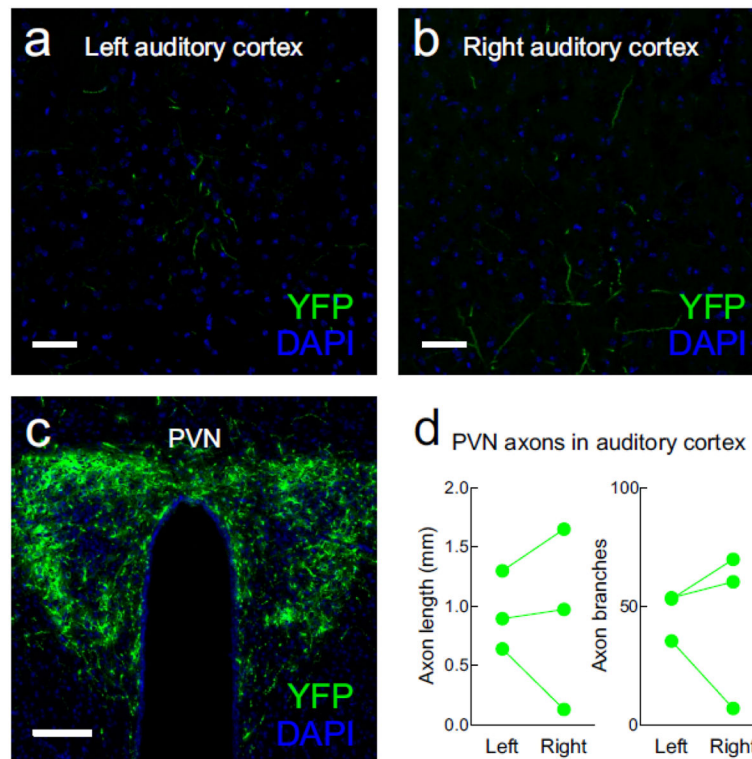
Extended Data Figure 4.
Oxytocinergic projections from hypothalamus to auditory cortex. We identified YFP-positive axon segments in sections from *Oxt-IRES-Cre* animals. **a**, Oxytocinergic projections in left auditory cortex. Green, YFP. Blue, DAPI. Scale, 100 μm. **b**, Oxytocinergic projections in right auditory cortex from same animal as in **a**. Scale, 100 μm. **c**, Oxytocinergic fibers and cells in PVN from same animal as in **a** and **b**. Scale, 100 μm. **d**, Quantification of axon segment length and number of axonal branches in left and right auditory cortex. No significant differences were found in total length or branch number in left vs. right cortex (left axon length: 0.94 ± 0.19 mm, right axon length: 0.92 ± 0.44 mm, n=3 mice, p>0.9, Student's paired two-tailed t-test; left: 47.3 ± 6.0 axon branches, right: 45.6 ± 19.6 axon branches, p>0.9).
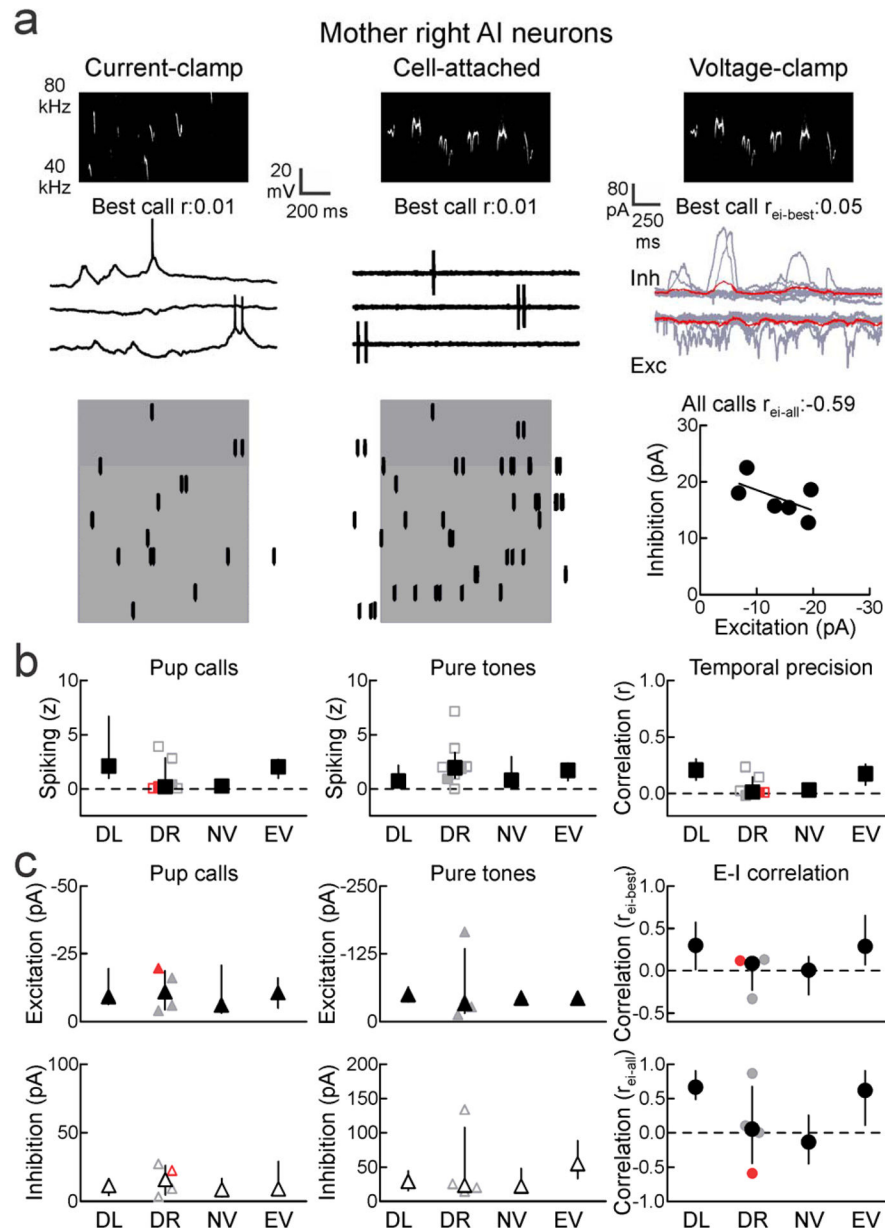
Extended Data Figure 5.

Spiking and synaptic pup call responses in dam right AI neurons. **a**, Three example recordings from right AI neurons of experienced mothers. Left, current-clamp recording. Top, spectrogram of best pup call; middle, three example traces evoked by this call; bottom, raster plot showing spikes evoked over 12 trials (spiking z-score: 0.2; trial-by-trial average correlation r: 0.01). Middle, cell-attached recording (spiking z-score: 0.1; trial-by-trial correlation r: 0.01). Right, voltage-clamp recording. IPSCs and EPSCs shown were evoked by the best pup call (gray, individual trials; red, average; $r_{ei\text{-}best}$: 0.05, $r_{ei\text{-}all}$: −0.59). **b**, Summary of spiking responses in dam right ('DR') AI neurons. Shown for comparison are responses from left AI neurons of dams ('DL'), naive virgins ('NV'), and experienced virgins ('EV') from Figure 4. Left, spiking responses to best pup calls (gray filled squares,

current-clamp; open gray squares, cell-attached recordings; black squares, median z-score: 0.2±0.8, n=7, p>0.7 compared to naive virgin responses with Wilcoxon-Mann-Whitney two-sample rank test with Bonferroni correction for multiple comparisons, U=76). Middle, spiking responses to pure tones (median z-score: 1.6±0.3, n=8, p>0.4 compared to naive virgin responses, U=83). Right, trial-by-trial correlation of pup call spiking responses (median r: 0.01±0.04, n=7, p>0.6 compared to naive virgin responses, U=78). Red squares indicate cells shown in **a**. **c**, Summary of synaptic responses in dam right AI neurons. Shown for comparison are responses from left AI neurons of dams, naive virgins, and experienced virgins from Figure 5. Top left, EPSCs evoked by best pup calls (median EPSC: −11.0±4.7, n=4, p>0.8 compared to naive virgin responses, U=60). Bottom left, IPSCs evoked by best pup calls (median IPSC: 16.0±7.0, n=4, p>0.4 compared to naive virgin responses, U=68). Top middle, EPSCs evoked by pure tones (median EPSC: −33.8±44.1, n=7, p>0.4 compared to naive virgin responses, U=52). Bottom middle, IPSCs evoked by pure tones (median IPSC: 22.9±35.7, n=7, p>0.7 compared to naive virgin responses, U=45). Top right, excitatory-inhibitory correlations in temporal profiles of best call responses (median $r_{ei\text{-}best}$: 0.08±0.14, n=4, p>0.7 compared to naive virgin responses, U=60). Bottom right, excitatory-inhibitory correlations across all calls (median $r_{ei\text{-}all}$: 0.05±0.37, n=4, p>0.8 compared to naive virgin responses, U=59). Red triangles indicate cell shown in **a**. Statistics are medians ± s.e.m. and error bars are medians ± interquartile range.
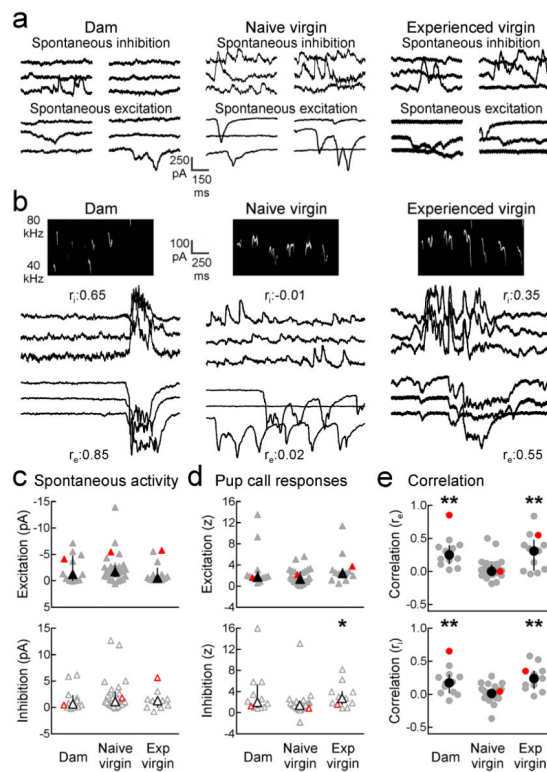
Extended Data Figure 6.
Pup call responses in experienced vs. naive females differ in timing but not overall amplitude. **a**, Example periods of spontaneous excitation and inhibition in absence of pup

call stimuli; same recordings as in Figure 5a. b, Example call-evoked IPSCs and EPSCs from left AI neurons; same recordings as in Figure 5a. Left column, neuron from dam. Top, spectrogram. Middle, IPSCs evoked by the best pup call (three individual trials are shown; average trial-by-trial correlation across all trials r_i: 0.65). Note similarity and shared temporal structure across individual trials in this cell. Bottom, EPSCs evoked by this call (r_e: 0.85). Middle column, neuron from naive virgin (r_i: −0.01; r_e: 0.02). Right column, neuron from experienced virgin (r_i: 0.35; r_e: 0.55). **c**, Summary of spontaneous excitation (top, filled triangles) and inhibition (bottom, open triangles) measured as instantaneous current (pA). Spontaneous activity was similar in left AI neurons from dams (black triangle, median excitation: −1.2±0.9 pA, n=13, p>0.7 compared to naive virgin spontaneous activity with Wilcoxon-Mann-Whitney two-sample rank test with Bonferroni correction for multiple comparisons, U=178; open triangle, median inhibition: 0.6±0.8 pA, p>0.3 compared to naive virgin responses, U=193), naive virgins (median excitation: −1.7±0.7 pA, n=28; median inhibition: 1.1±0.8 pA), and experienced virgins ('Exp virgin', median excitation: −0.6±0.7 pA, n=13, p>0.1 compared to naive virgin spontaneous activity, U=232; median inhibition: 1.3±0.7 pA, p>0.5 compared to naive virgin responses, U=168). Red triangles indicate cells shown in **a** and **b. d**, Summary of z-scored call-evoked EPSCs (top) and IPSCs (bottom) relative to spontaneous activity in dams (filled triangle, median excitation z-score: 1.8±1.4, n=13, p>0.1 compared to naive virgin responses, U=215; open triangle, median inhibition z-score: 2.0±1.6, p>0.1 compared to naive virgin responses, U=181), naive virgins (median excitation z-score: 1.4±0.3, n=28; median inhibition z-score: 1.4±0.6), and experienced virgins (median excitation z-score: 2.5±1.0, n=13, p>0.1 compared to naive virgin responses, U=250; median inhibition z-score: 2.7±0.9, p<0.02 compared to naive virgin responses, U=228). Red triangles indicate cells shown in **a** and **b. e**, Summary of trial-by-trial correlations in temporal profile of best call responses for EPSCs (top, r_e) and IPSCs (bottom, r_i) for dams (r_e: 0.25±0.08, n=12, p<10^{-4} compared to naive virgin responses, U=294; r_i: 0.18±0.08, p<0.01 compared to naive virgin responses, U=230), naive virgins (r_e: 0.0±0.03, n=28; r_i: 0.01±0.03), and experienced virgins (r_e: 0.31±0.09, n=13, p<0.007 compared to naive virgin responses, U=285; r_i: 0.24±0.07, p<0.001 compared to naive virgin responses, U=233). Red circles indicate cells shown in **a** and **b**. *, p<0.05, **, p<0.01. Statistics are medians ± s.e.m. and error bars are medians ± interquartile range.
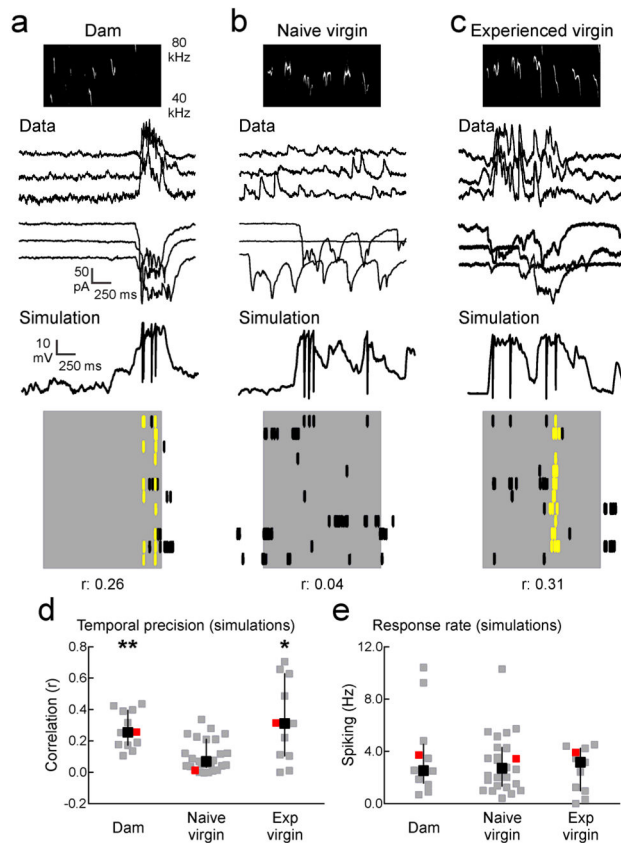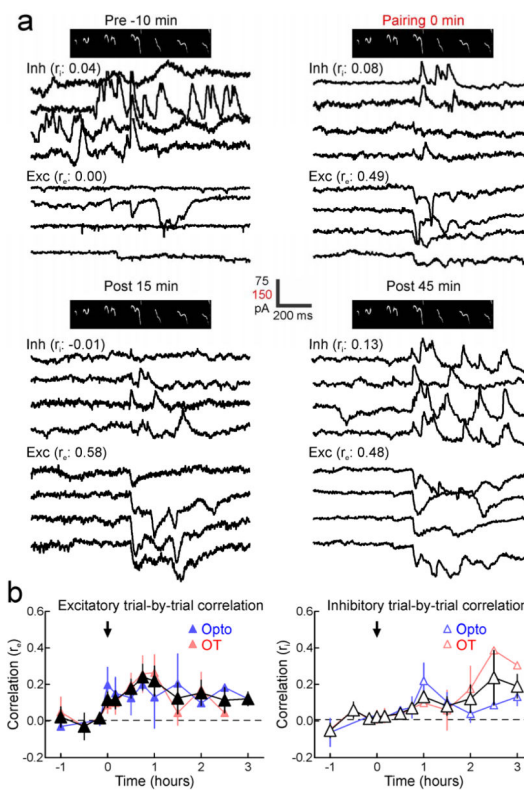
Extended Data Figure 7.

Simulations of spikes predicted from currents measured in voltage-clamp recordings. **a**, Neuron from dam left AI (same cell as in Fig. 5a, left). Top, experimental data. Three representative EPSCs and three IPSCs evoked by the best call are displayed. Bottom, results of simulation. The membrane potential and spikes (clipped for display) of one trial run is shown, with a raster plot of 12 trials below. Yellow events indicate spikes that are synchronous within ~10 msec on 50%+ trials. There was a high trial-to-trial correlation in spike firing (r: 0.26). **b**, Neuron from naive virgin left AI (same cell as in Fig. 5a, middle). Simulations using currents recorded in this cell predicted a low trial-to-trial correlation (r: 0.04). **c**, Neuron from experienced virgin left AI (same cell as in Fig. 5a, right). Simulations predicted a high trial-to-trial correlation (r: 0.31). **d**, Summary of simulated trial-by-trial spiking correlations for all voltage-clamp recordings from Figure 5 of dams (median r: 0.25±0.04, n=12, p<0.0004 compared to simulated naive virgin responses with Wilcoxon-Mann-Whitney two-sample rank test with Bonferroni correction for multiple comparisons, U=269), naive virgins (median r: 0.07±0.02, n=26), and experienced virgins (median r: 0.31±0.10, n=11, p<0.04 compared to simulated naive virgin responses, U=213). Red squares indicate cells shown in **a**–**c**. Note similarity to spike timing correlations measured experimentally and shown in Figure 4e. **, p<0.01; *, p<0.05. **e**, Summary of simulated call-evoked firing rates of dams (median: 2.5±1.1 Hz, n=12, p>0.8 compared to naive virgin responses, U=161), naive virgins (median: 2.7±0.5 Hz, n=23), and experienced virgins (median: 3.2±0.6 Hz, n=11, p>0.6 compared to naive virgin responses, U=157). The

simulated call-evoked responses were similar across each group due to the normalization of evoked current amplitudes; normalizing peak EPSCs and IPSCs allowed us to examine changes in spike timing independently from changes in overall spike rate. Statistics are medians ± s.e.m. and error bars are medians ± interquartile range.
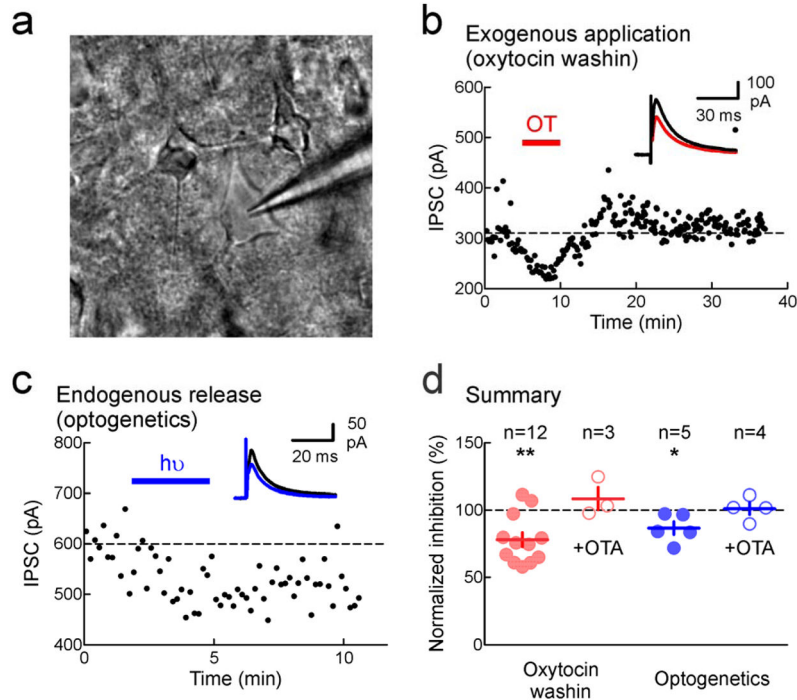
Extended Data Figure 8.
Oxytocin receptor activation disinhibits cortical neurons in brain slices. **a**, Photomicrograph showing whole-cell recording from layer 5 pyramidal neuron in brain slice of virgin female mouse auditory cortex. **b**, Example voltage-clamp recording of IPSCs evoked by extracellular stimulation. Oxytocin ('OT') was washed into the bath for 5 minutes. Red bar, duration of oxytocin washin. Dashed line, baseline IPSC amplitude. **, p<0.01. Inset, IPSCs before (black) and 3–5 minutes after washin (red). **c**, Example voltage-clamp recording of IPSCs evoked by extracellular stimulation in brain slice from *Oxt-IRES-Cre* mouse expressing ChETA in oxytocin neurons. Oxytocin release was evoked by blue light ('hυ') for three minutes. *, p<0.05. **d**, Summary of changes to evoked IPSCs 3–5 minutes after oxytocin receptor activation, by exogenous oxytocin washin (red; 78.0±5.3% of baseline amplitude; n=12, p<0.002 compared to baseline; prevented by OTA, 108.6±8.6% of baseline amplitude; n=3, p>0.4 compared to baseline) or by optogenetic release of endogenous oxytocin (86.7±4.7% of baseline amplitude; n=5, p<0.05 compared to baseline; prevented by OTA, 101.2±1.2% of baseline amplitude; n=4, p>0.8 compared to baseline). Statistics and error bars are means± s.e.m.

Extended Data Figure 9.
Oxytocin pairing increases the trial-by-trial similarity of synaptic pup call responses. **a** Same voltage-clamp recording from virgin female left AI neuron as in Figure 6c, showing that trial-by-trial similarity of call-evoked IPSCs and EPSCs is initially low but increases after oxytocin pairing. Shown are four representative IPSCs and EPSCs before pairing (inhibitory trial-by-trial correlation r_i: 0.04, excitatory trial-by-trial correlation r_e: 0.00), during pairing (r_i: 0.08, r_e: 0.49), 10–15 minutes after pairing (r_i: −0.01, r_e: 0.58), and 45–50 minutes after pairing (r_i: 0.13, r_e: 0.48). Scale: 75 pA (150 pA during pairing), 200 msec. **b**, Summary of changes to synaptic trial-by-trial correlations after oxytocin pairing in virgin left AI. Left, change in excitatory correlations (r_e) across multiple cells for hours after pairing. Blue, optogenetic pairing ('opto'); red, oxytocin pairing ('OT'); black, means binned over time (n=28 cells from 17 animals; r_e before pairing: 0.01±0.02, r_e 0–45 minutes after pairing: 0.16±0.03, p<0.0002 compared to values before pairing; r_e 1–3 hours after pairing: 0.16±0.04, p<0.0009 compared to values before pairing). Dashed line, initial average r_e; arrow, time of pairing. Right, change in r_i (r_i before pairing: 0.01±0.02, r_i 0–45 minutes after pairing: 0.04±0.02, p>0.1 compared to values before pairing; r_i 1–3 hours after pairing: 0.14±0.03, p<0.0002 compared to values before pairing). Statistics and error bars are means ± s.e.m.

Supplementary Material

Refer to Web version on PubMed Central for supplementary material.

Acknowledgments

References

1. Richard P, Moos F, Freund-Mercier MJ. Central effects of oxytocin. Physiol Rev. 1991; 71:331–370. [PubMed: 1672455]

2. Gimpl G, Fahrenholz F. The oxytocin receptor system: structure, function, and regulation. Physiol Rev. 2001; 81:629–683. [PubMed: 11274341]

3. Insel TR, Young LJ. The neurobiology of attachment. Nat Rev Neurosci. 2001; 2:129–136. [PubMed: 11252992]

4. Insel TR. The challenge of translation in social neuroscience: a review of oxytocin, vasopressin, and affiliative behavior. Neuron. 2010; 65:768. [PubMed: 20346754]

5. Bartz JA, Zaki J, Bolger N, Ochsner KN. Social effects of oxytocin in humans: Context and person matter. Trends Cogn Sci. 2011; 15:301–309. [PubMed: 21696997]

6. Churchland PS, Winkielman P. Modulating social behavior with oxytocin: how does it work? What does it mean? Horm Behav. 2012; 61:392–399. [PubMed: 22197271]

7. Pedersen CA, Ascher JA, Monroe YL, Prange AJ. Oxytocin induces maternal behavior in virgin female rats. Science. 1982; 216:648–650. [PubMed: 7071605]

8. Winslow JT, Insel TR. Social status in pairs of male squirrel monkeys determines the behavioral response to central oxytocin administration. J Neurosci. 1991; 11:2032–2038. [PubMed: 1648603]

9. Nishimori K, et al. Oxytocin is required for nursing but is not essential for parturition or reproductive behavior. Proc Natl Acad Sci U S A. 1996; 93:11699–11704. [PubMed: 8876199]

10. Zak PJ, Stanton AA, Ahmadi S. Oxytocin increases generosity in humans. PLoS One. 2007; 2:e1128. [PubMed: 17987115]

11. Andari E, et al. Promoting social behavior with oxytocin in high-functioning autism spectrum disorders. Proc Natl Acad Sci U S A. 2010; 107:4389–4394. [PubMed: 20160081]

12. Chang SW, Platt ML. Oxytocin and social cognition in rhesus macaques: Implications for understanding and treating human psychopathology. Brain Res. 2014; 1580:57–68. [PubMed: 24231551]

13. Dulac C, O'Connell LA, Wu Z. Neural control of maternal and paternal behaviors. Science. 2014; 345:765–770. [PubMed: 25124430]

14. Rilling JK, Young LJ. The biology of mammalian parenting and its effects on offspring social development. Science. 2014; 345:771–776. [PubMed: 25124431]

15. Yoshida M, et al. Evidence that oxytocin exerts anxiolytic effects via oxytocin receptor expressed in serotonergic neurons in mice. J Neurosci. 2009; 29:2259–2271. [PubMed: 19228979]

16. Nakajima M, Görlich A, Heintz N. Oxytocin modulates female sociosexual behavior through a specific class of prefrontal cortical interneurons. Cell. 2014; 159:295–305. [PubMed: 25303526]

17. Sewell GD. Ultrasonic communication in rodents. Nature. 1970; 227:410. [PubMed: 5464098]

18. Noirot E. Ultrasounds and maternal behavior in small rodents. Dev Psychobiol. 1972; 5:371–387. [PubMed: 4609822]

19. Ehret G. Left hemisphere advantage in the mouse brain for recognizing ultrasonic communication calls. Nature. 1987; 325:249–251. [PubMed: 3808021]

20. Fichtel I, Ehret G. Perception and recognition discriminated in the mouse auditory cortex by c-Fos staining. NeuroReport. 1999; 10:2341–2345. [PubMed: 10439460]

21. Ehret G. Infant rodent ultrasounds- a gate to the understanding of sound communication. Behav Genet. 2005; 35:19–29. [PubMed: 15674530]

22. Crawley JN. Behavioral phenotyping strategies for mutant mice. Neuron. 2008; 57:809–818. [PubMed: 18367082]

23. Cohen L, Rothschild G, Mizrahi A. Multisensory integration of natural odors and sounds in the auditory cortex. Neuron. 2011; 72:357–369. [PubMed: 22017993]

24. Hofstetter KM, Ehret G. The auditory cortex of the mouse: connections of the ultrasonic field. J Comp Neurol. 1992; 323:370–386. [PubMed: 1460109]

25. Liu RC, Linden JF, Schreiner CE. Improved cortical entrainment to infant communication calls in mothers compared with virgin mice. Eur J Neurosci. 2006; 23:3087–3097. [PubMed: 16819999]

26. Liu RC, Schreiner CE. Auditory cortical detection and discrimination correlates with communicative significance. PLoS Biol. 2007; 5:173.

27. Rothschild G, Cohen L, Mizrahi A, Nelken I. Elevated correlations in neuronal ensembles of mouse auditory cortex following parturition. J Neurosci. 2013; 33:12851–12861. [PubMed: 23904620]

28. Koch M, Ehret G. Estradiol and parental experience, but not prolactin are necessary for ultrasound recognition and pup-retrieving in the mouse. Physiol Behav. 1989; 45:771–776. [PubMed: 2780846]

29. Irani BG, et al. Distribution and neurochemical characterization of protein kinase C-theta and -delta in the rodent hypothalamus. Neuroscience. 2010; 170:1065–1079. [PubMed: 20691763]

30. Wu Z, et al. An obligate role of oxytocin neurons in diet induced energy expenditure. PLoS One. 2012; 7:e45167. [PubMed: 23028821]

31. Knobloch HS, et al. Evoked axonal oxytocin release in the central amygdala attenuates fear response. Neuron. 2012; 73:553–566. [PubMed: 22325206]

32. Takayanagi Y, et al. Pervasive social deficits, but normal parturition, in oxytocin receptor-deficient mice. Proc Natl Acad Sci U S A. 2005; 102:16096–16101. [PubMed: 16249339]

33. Gong S, et al. A gene expression atlas of the central nervous system based on bacterial artificial chromosomes. Nature. 2003; 425:917–925. [PubMed: 14586460]

34. Wehr M, Zador AM. Balanced inhibition underlies tuning and sharpens spike timing in auditory cortex. Nature. 2003; 426:442–446. [PubMed: 14647382]

35. Tan AY, Wehr M. Balanced tone-evoked synaptic excitation and inhibition in mouse auditory cortex. Neuroscience. 2009; 163:1302–1315. [PubMed: 19628023]

36. Dorrn A, Yuan K, Barker AJ, Schreiner CE, Froemke RC. Developmental sensory experience balances cortical excitation and inhibition. Nature. 2010; 465:932–936. [PubMed: 20559387]

37. Froemke RC, Merzenich MM, Schreiner CE. A synaptic memory trace for cortical receptive field plasticity. Nature. 2007; 450:425–429. [PubMed: 18004384]

38. Kruglikov I, Rudy B. Perisomatic GABA release and thalamocortical integration onto neocortical excitatory cells are regulated by neuromodulators. Neuron. 2008; 58:911–924. [PubMed: 18579081]

39. Letzkus JJ, et al. A disinhibitory microcircuit for associative fear learning in the auditory cortex. Nature. 2011; 480:331–335. [PubMed: 22158104]

40. Froemke RC, et al. Long-term modification of cortical synapses improves sensory perception. Nat Neurosci. 2013; 16:79–88. [PubMed: 23178974]

41. Owen SF, et al. Oxytocin enhances hippocampal spike transmission by modulating fast-spiking interneurons. Nature. 2013; 500:458–462. [PubMed: 23913275]

42. Rudick CN, Woolley CS. Estrogen regulates functional inhibition of hippocampal CA1 pyramidal cells in the adult female rat. J Neurosci. 2001; 21:6532–6543. [PubMed: 11517242]

43. Loring DW, et al. Cerebral language lateralization: evidence from intracarotid amobarbital testing. Neuropsychologia. 1990; 28:831–838. [PubMed: 2247209]

44. Bishop DV. Cerebral asymmetry and language development: cause, correlate, or consequence? Science. 2013; 340:1230531. [PubMed: 23766329]

45. Yoon H, Enquist LW, Dulac C. Olfactory inputs to hypothalamic neurons controlling reproduction and fertility. Cell. 2005; 123:669–682. [PubMed: 16290037]

46. Fraser EJ, Shah NM. Complex chemosensory control of female reproductive behaviors. PLoS One. 2014; 9:e90368. [PubMed: 24587340]

47. Wacker DW, Ludwig M. Vasopressin, oxytocin, and social odor recognition. Horm Behav. 2012; 61:259–265. [PubMed: 21920364]

48. Lin D, et al. Functional identification of an aggression locus in the mouse hypothalamus. Nature. 2011; 470:221–226. [PubMed: 21307935]

49. Bennur S, Tsunada J, Cohen YE, Liu RC. Understanding the neurophysiological basis of auditory abilities for social communication: a perspective on the value of ethological paradigms. Hear Res. 2013; 305:3–9. [PubMed: 23994815]

50. Wu Z, Autry AE, Bergan JF, Watabe-Uchida M, Dulac CG. Galanin neurons in the medial preoptic area govern parental behavior. Nature. 2014; 509:325–330. [PubMed: 24828191]

51. Huber D, Veinante P, Stoop R. Vasopressin and oxytocin excite distinct neuronal populations in the central amygdala. Science. 2005; 308:245–248. [PubMed: 15821089]

52. Dölen G, Darvishzadeh A, Huang KW, Malenka RC. Social reward requires coordinated activity of nucleus accumbens oxytocin and serotonin. Nature. 2013; 501:179–184. [PubMed: 24025838]

53. Gunaydin LA, Yizhar O, Berndt A, Sohal VS, Deisseroth K, Hegemann P. Ultrafast optogenetic control. Nat Neurosci. 2010; 13:387–392. [PubMed: 20081849]

54. Kubota Y, et al. Structure and expression of the mouse oxytocin receptor gene. Mol Cell Endocrinol. 1996; 124:25–32. [PubMed: 9027321]

55. Harris JA, et al. Anatomical characterization of Cre driver mice for neural circuit mapping and manipulation. Front Neural Circuits. 2014; 8:76. [PubMed: 25071457]

56. Fellous JM, Tiesinga PH, Thomas PJ, Sejnowski TJ. Discovering spike patterns in neuronal responses. J Neurosci. 2004; 24:2989–3001. [PubMed: 15044538]
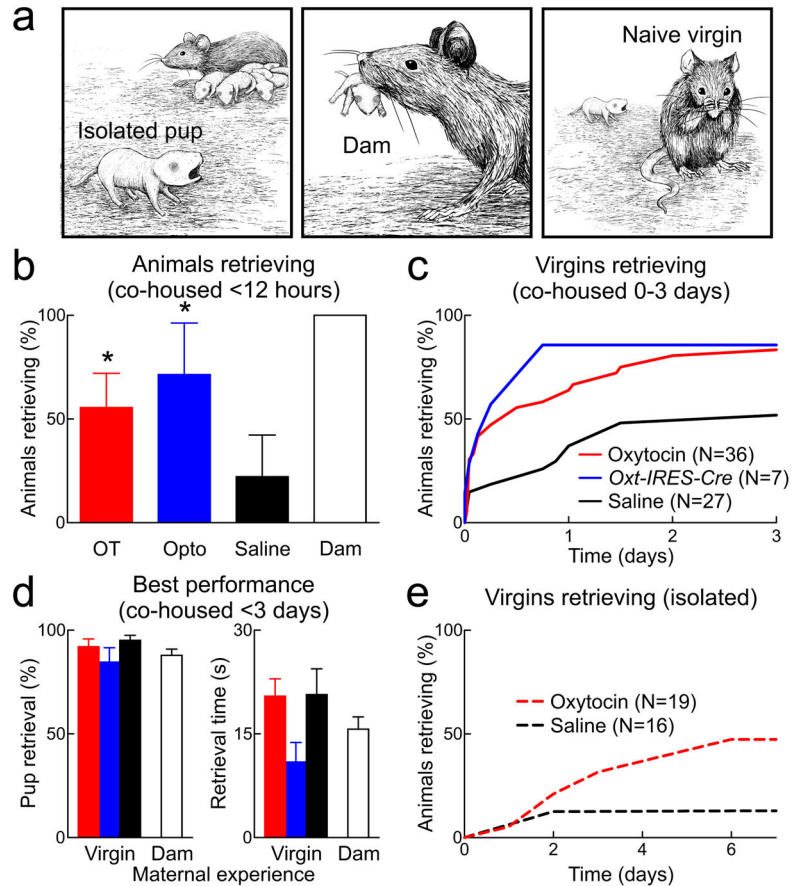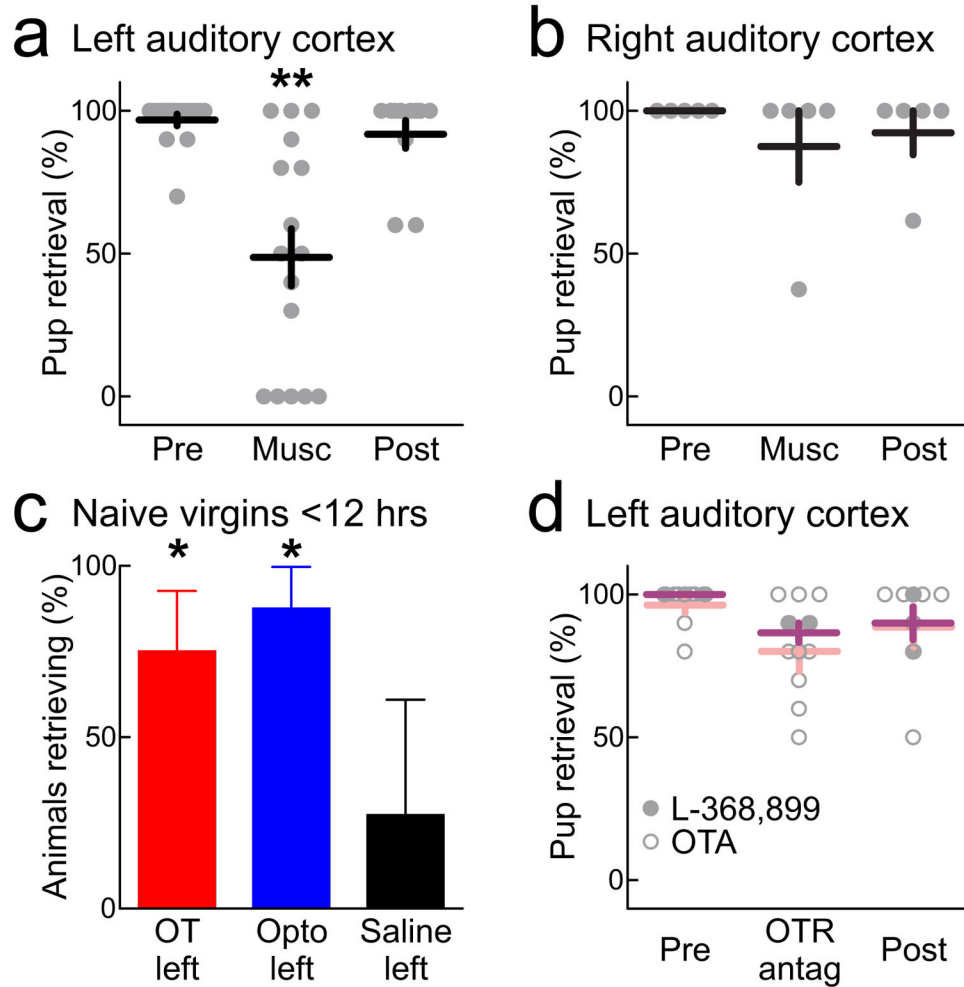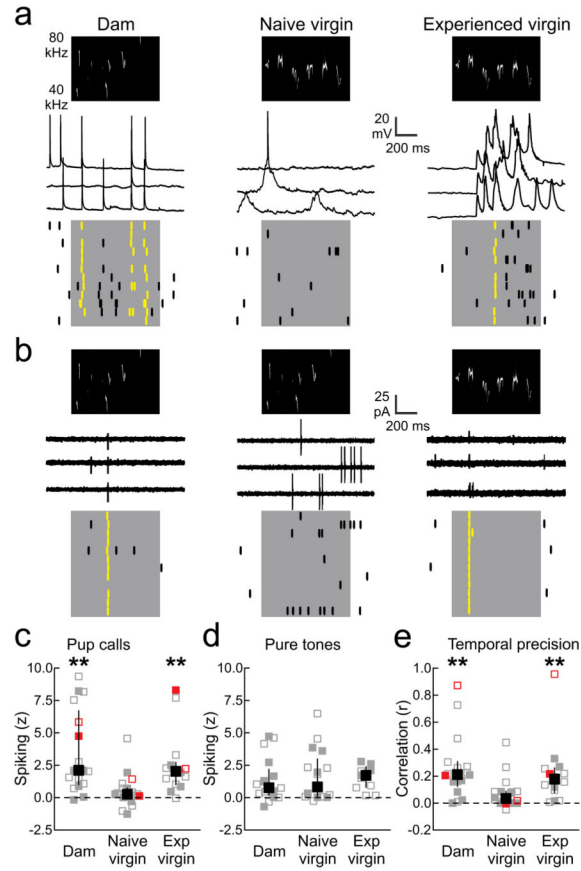
Figure 1.
Oxytocin enables pup retrieval. **a**, Retrieval behavior. **b**, Initially-naive virgins retrieving 1+ times <12 hours after co-housing (oxytocin: 20/36 animals, p<0.03; optogenetic PVN stimulation: 5/7 animals, p<0.05; saline: 6/27 animals). *, p<0.05. Error bars:means±95% confidence intervals. **c**, Cumulative retrieval during co-housing. **d**, Retrieval rates (p>0.5) and speed (p>0.1) were similar in dams and experienced virgins. Error bars:means±s.e.m. **e**, Cumulative retrieval of saline-injected (N=16) or oxytocin-injected (N=19) isolated virgins (2 days post-testing, saline: 2/16 animals retrieved, oxytocin: 4/19 animals, p>0.6; 6 days, saline: 2/16 animals, oxytocin: 9/19 animals, p<0.03).
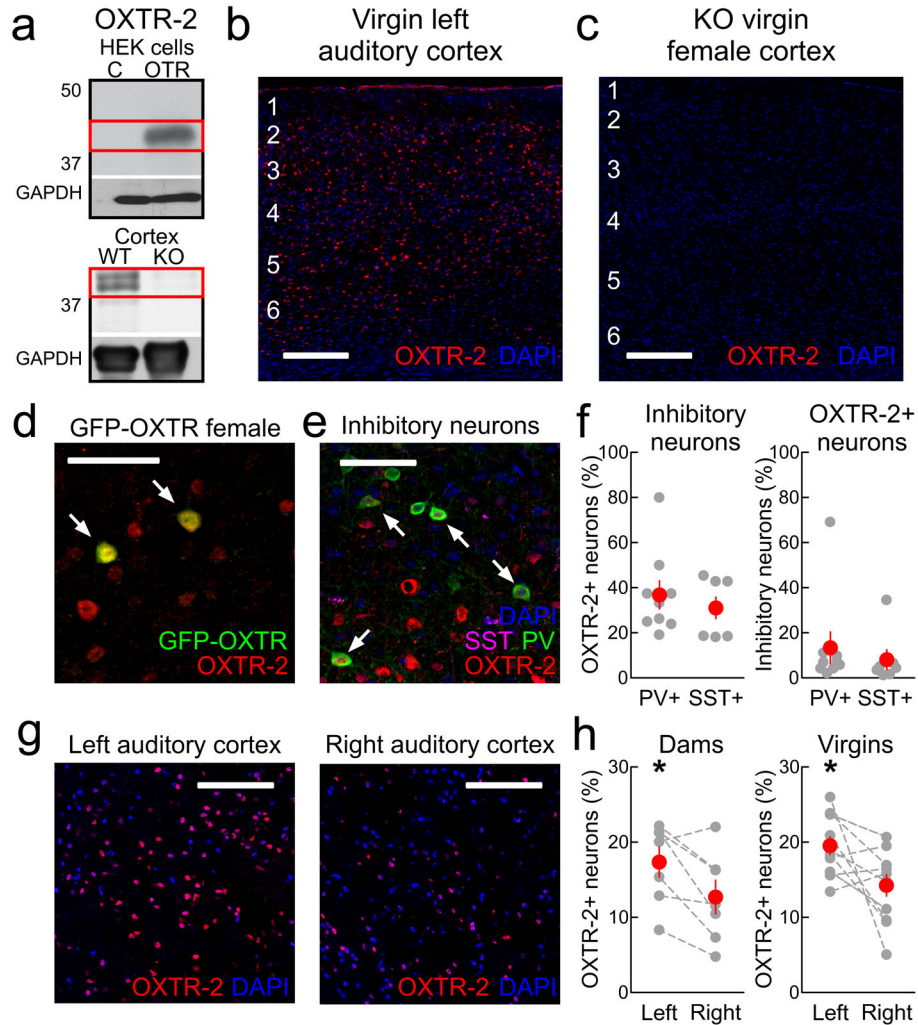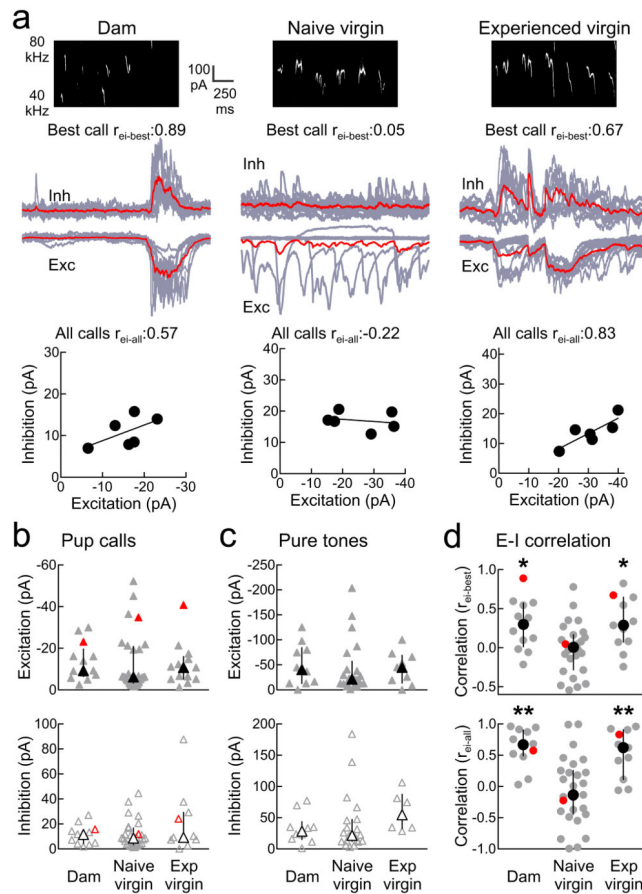
Figure 2.
Oxytocin receptor expression in female auditory cortex. **a**, Antibody to mouse oxytocin receptor (OXTR-2). Top, immmunoblot of HEK cells expressing oxytocin receptors ('OTR') vs. control ('C'). Bottom, OXTR-2 immunoblots of cortical lysates from wild-type ('WT'), knockout animals ('KO'). Red, oxytocin receptor molecular weight (43 kD). GAPDH, loading controls. **b**, Immunostaining in left auditory cortex of naïve virgin. Scale: 150 μm. **c**, No labeling in oxytocin receptor knockouts. Scale: 150 μm. **d**, Left auditory cortex of eGFP-oxytocin receptor virgin co-stained for eGFP. Arrows, double-labeled cells. Scale: 50 μm. **e**, Cortical interneurons express oxytocin receptors. Virgin left auditory cortex layer 5 co-stained for parvalbumin/somatostatin. Scale: 50 μm. **f**, Co-labeled OXTR-2+ and PV+/SST+ auditory cortical cells. **g**, Left, right auditory cortex from same naive virgin. Scale: 100 μm. **h**, Oxytocin receptors expressed more in left auditory cortex (mothers, left: 17.4±2.0%, right: 12.7±2.4%, left/right asymmetry: 37.0%, p<0.03, N=7; virgins, left: 19.5±1.2%, right: 14.3±1.4%, asymmetry: 36.4%, p<0.02, N=12). Statistics, error bars:means±s.e.m.
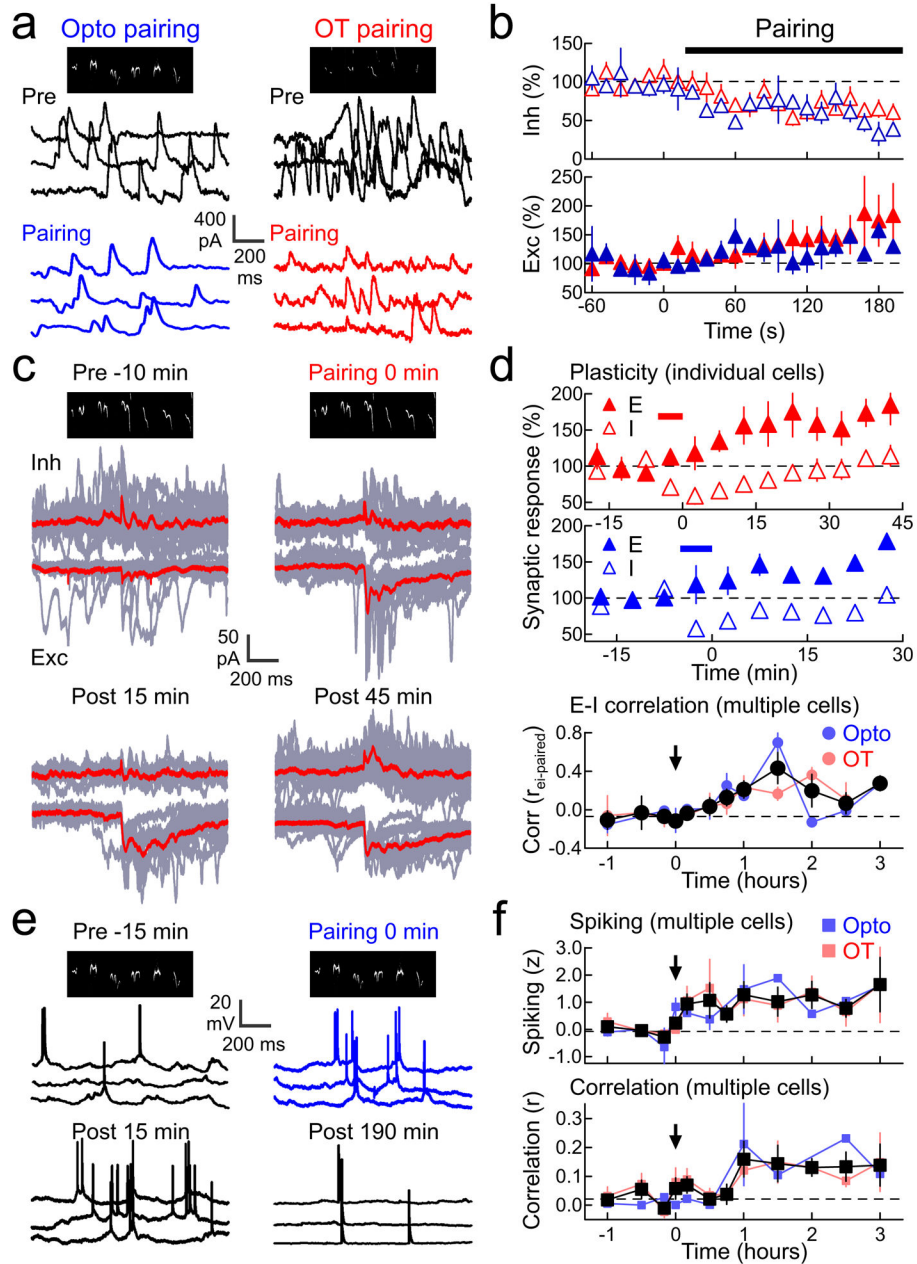
Figure 3.
Oxytocin receptors in left auditory cortex are initially required for retrieval. **a**, Muscimol infused into left AI reduced retrieval by experienced animals (pre-muscimol retrieval: 96.9±2.0%, 16/16 animals retrieving 1+ times; muscimol: 48.8±10.0%, p<0.002, 11/16 animals retrieving, p<0.025). **, p<0.01. Statistics, error bars:means±s.e.m. **b**, Muscimol in right AI did not impair retrieval (pre-muscimol: 100.0±0.0%, muscimol: 87.5±12.5%, p>0.9; 5/5 animals retrieved). **c**, Oxytocin in left AI of naive virgins accelerated time to first retrieval <12 hours of co-housing (oxytocin: 12/16 animals, p<0.05; optogenetic stimulation: 7/8 animals, p<0.04; saline: 3/11 animals). Error bars:means±95% confidence intervals. **d**, Retrieval of experienced animals with OTA (baseline: 96.3±2.6%, OTA: 80.0±6.8%, p>0.05; 8/8 animals) or L-368,899 (baseline: 100.0±0.0%, L-368,899: 86.7±3.3%, p>0.1, N=3; 3/3 animals) infused into left AI.

Figure 4.
Pup calls evoke reliable spikes in experienced female left AI. **a**, Current-clamp recordings in left AI of dam (spiking z-score: 4.7; trial-by-trial average correlation r: 0.21), naive virgin (z-score: 0.1; r:−0.04), experienced virgin (z-score: 8.3; r: 0.27). **b**, Cell-attached recordings from dam (z-score: 5.8; r: 0.87), naive virgin (z-score: 1.4; r: 0.04), experienced virgin (z-score: 2.1; r: 0.96). **c**, Current-clamp (filled) or cell-attached (open) call-evoked responses in dams (black, z-score: 2.1±1.0, n=17, p<0.0004, U=288), naive virgins (z-score: 0.2±0.3, n=20), experienced virgins (z-score: 2.0±0.8, n=14, p<0.006, U=240). Statistics:medians ±s.e.m.; error bars: medians±interquartile range. **d**, Tone-evoked responses in left AI of dams (z-score: 0.7±0.5, n=17, p>0.7, U=154), naive virgins (z-score: 0.8±0.6, n=17), experienced virgins (z-score: 1.7±0.4, n=11, p>0.6, U=105). **e**, Trial-by-trial correlation in dams (r: 0.21±0.07, n=17, p<0.002, U=276), naive virgins (r: 0.03±0.03, n=20), experienced virgins (r: 0.18±0.08, n=14, p<0.012, U=219). Red, cells in **a**, **b**.

Figure 5.
Pup calls evoke correlated patterns of excitatory and inhibitory responses in left AI of experienced females. **a**, Voltage-clamp recordings from dam (top, best call responses, $r_{ei-best}$: 0.89; bottom, IPSCs and EPSCs across calls, r_{ei-all}: 0.57), naive virgin ($r_{ei-best}$: 0.05; r_{ei-all}:−0.22), experienced virgin ($r_{ei-best}$: 0.67; r_{ei-all}: 0.83). **b**, Synaptic call-evoked responses from dams (excitation:−9.3±3.1 pA, n=13, p>0.3, U=229; inhibition: 11.6±2.8 pA, p>0.5, U=182), naive virgins (excitation:−6.2±3.3 pA, n=28; inhibition: 8.7±2.7 pA), experienced virgins (excitation:−10.8±3.6 pA, n=13, p>0.6, U=205; inhibition: 9.2±9.5 pA, p>0.4, U=171). Red, cells in **a**. Statistics:medians±s.e.m.; error bars: medians±interquartile range. **c**, Tone-evoked responses in dams (excitation:−40.6±16.7 pA, n=10, p>0.4, U=123; inhibition: 28.7±9.6 pA, p>0.7, U=108), naive virgins (excitation:−21.6±14.8 pA, n=21; inhibition: 21.8±13.2 pA), experienced virgins (excitation:−45.2±13.8 pA, n=9, p>0.5, U=107; inhibition: 54.7±16.4 pA, p>0.1, U=92). **d**, Excitatory-inhibitory correlation of best call responses (top, $r_{ei-best}$) and across all calls (bottom, r_{ei-all}) dams ($r_{ei-best}$: 0.30±0.12, n=12, p<0.03, U=245; r_{ei-all}: 0.67±0.11, p<0.0004, U=278), naive virgins ($r_{ei-best}$: 0.00±0.08, n=27; r_{ei-all}:−0.13±0.13), experienced virgins ($r_{ei-best}$: 0.29±0.13, n=12, p<0.03, U=224; r_{ei-all}: 0.62±0.14, p<0.006, U=236).

Figure 6.

Oxytocin pairing modifies excitatory-inhibitory balance. **a**, Call-evoked IPSCs from virgin left AI neuron before/during optogenetic (blue) or oxytocin pairing (red). **b**, Oxytocin reduced inhibition within 40–60 seconds (top; optogenetic pairing, n=4, p<0.002; oxytocin pairing, n=12, p<0.04). **c**, Voltage-clamp recording from virgin left AI neuron (pre-pairing IPSCs: 8.3±1.1 pA, pre-pairing EPSCs:−8.0±1.2 pA, $r_{ei-paired}$: 0.13; pairing IPSCs: 6.5±1.5 pA, EPSCs:−10.4±3.0 pA, $r_{ei-paired}$:−0.12; 10–15 minutes post-pairing IPSCs: 4.9±0.9 pA, p<0.0009, EPSCs:−15.4±1.3 pA, p<0.005, $r_{ei-paired}$:−0.14; 45–50 minutes post-pairing IPSCs: 9.6±2.1 pA, p>0.5, EPSCs:−13.4±2.4 pA, p<0.002, $r_{ei-paired}$: 0.27). Statistics, error bars:means±s.e.m. **d**, Synaptic modifications. Top, individual neurons after oxytocin (EPSC

increase: 43.5±15.7%, n=10, p<0.03; IPSC decrease:−33.7±7.8%, p<0.004) or optogenetic pairing (EPSC increase: 47.5±13.2%, n=6, p<0.02; IPSC decrease:−20.0±4.3%, p<0.02). Bottom, excitatory-inhibitory correlation (n=28 cells, 17 animals; $r_{ei-paired}$ pre-pairing: −0.07±0.05, $r_{ei-paired}$ 0–45 minutes post-pairing: 0.02±0.04, p>0.1; $r_{ei-paired}$ 1–3 hours post-pairing: 0.24±0.06, p<0.0002). **e**, Two current-clamp recordings from same virgin; first cell before optogenetic pairing (z-score: 0.04, r: 0.01), during pairing (z: 0.51, r: 0.00), 10–15 minutes post-pairing (z: 0.57, r: 0.03); second cell 180–190 minutes post-pairing (z: 1.60, r: 0.11). **f**, Spiking. Top, call-evoked spiking (n=28 cells, 13 animals; z-score pre-pairing: −0.13±0.11, 0–45 minutes post-pairing: 0.91±0.27, p<0.003; z-score 1–3 hours post-pairing: 1.21±0.25, p<10^{-4}). Bottom, trial-by-trial correlation (pre-pairing r: 0.01±0.01; 0–45 minutes post-pairing: 0.05±0.02, p>0.1; 1–3 hours post-pairing: 0.14±0.03, p<10^{-4}).